MHD simulations of flows around rotating and non-rotating axisymmetric magnetic flux concentrations

By T. Hartlep, F. H. Busse†, N. E. Hurlburt‡ AND A. G. Kosovichev

We present results on modeling magnetic flux tubes in an unstably stratified medium and the flows around them using 2D axisymmetric magneto-hydrodynamic (MHD) simulations. The study is motivated by the formation of magnetic field concentrations at the solar surface in sunspots and magnetic pores and the large-scale flow patterns associated with them. The simulations provide consistent, self-maintained models of concentrated magnetic field in a convective environment, although they are not fully realistic or directly applicable to the solar case. In this paper, we explore under which conditions the associated flows near the surface are converging (towards the spot center) or diverging (away from the axis) in nature. It is found that, depending on the parameters of the problem, the results can depend on the initial conditions, in particular for zero or low rotation rates and Prandtl numbers smaller than unity. The solutions with a converging flow usually produce more strongly confined magnetic flux tubes.

1. Motivation and Objectives

The mechanisms of how magnetic pores and sunspots form on the Sun are still poorly understood. Observations and numerical simulations suggest that their structure is intimately linked with characteristic surface and subsurface flows in and around the region of magnetic field concentration. Fully developed sunspots exhibit a surface outflow in their penumbra, the so-called Evershed flow, presumed to be caused by interaction between the near-surface granular convection and the highly inclined penumbral magnetic field as suggested by Hurlburt *et al.* (1996) and the numerical simulations of Kitiashvili *et al.* (2009). Observation (*e.g.*, Zhao *et al.* 2010) have revealed downflows in the central region of the sunspot and subsurface converging flows (inflows) below the granulation layer, as well as outflows further below. The inflows around magnetic structures without penumbra were also obtained in the realistic MHD simulations of Rempel *et al.* (2009) and Kitiashvili *et al.* (2010). It is conjectured that this flow is fundamentally important for maintaining the integrity of the magnetic field concentration.

These problems are the motivation for the present study but we do not try to closely approximate solar conditions here. Simplified numerical models of subsurface magneto-convection in axisymmetric configuration (Hurlburt & Rucklidge 2000; Botha *et al.* 2006, 2008) have been able to reproduce flow structures similar to those discussed above and Botha *et al.* (2008) did in fact also find cases with a diverging flow over a converging flow. The present paper extends their work, exploring in more detail the conditions under under which diverging or converging flows can hold a magnetic flux concentration in place.

† Institute of Physics, University of Bayreuth, Germany
‡ Lockheed Martin Solar and Astrophysics Laboratory, Palo Alto, California

2. Numerical method

We study magneto-convection in an axisymmetric cylindrical geometry using a code originally developed by Hurlburt & Rucklidge (2000) for the two-dimensional (2D) case and later extended by Botha *et al.* (2008). The model considers a layer of electrically conducting, perfect monatomic gas subject to uniform gravitational acceleration, with constant shear viscosity, magnetic diffusivity, and magnetic permeability, rotating with constant angular velocity Ω about the vertical. The model approximates the conditions in the upper part of the solar convection zone but excludes the granulation layer, the very top few hundred kilometers below the photosphere where the plasma is only partially ionized and radiation would need to be modeled accurately.

The equations in non-dimensional form read:

$$\partial_t \rho = -\nabla \cdot (\boldsymbol{u}\rho)\,, \tag{2.1}$$

$$\partial_t \boldsymbol{u} = -\boldsymbol{u}\cdot\nabla\boldsymbol{u} - 2\Omega\hat{\boldsymbol{z}}\times\boldsymbol{u} + \Omega^2(\hat{\boldsymbol{z}}\times\boldsymbol{r})\times\hat{\boldsymbol{z}} - \frac{1}{\rho}\nabla P + \theta(m+1)\hat{\boldsymbol{z}} + \frac{\sigma K}{\rho}\nabla\cdot\tau + \frac{\sigma K^2 Q\zeta_0}{\rho}\boldsymbol{j}\times\boldsymbol{B}, \tag{2.2}$$

$$\partial_t T = -\boldsymbol{u}\cdot\nabla T - (\gamma-1)T\nabla\cdot\boldsymbol{u} + \frac{\gamma K}{\rho}\nabla^2 T + \frac{\sigma K(\gamma-1)}{\rho}\left(\frac{1}{2}\tau:\tau + \zeta_0^2 Q K^2 j^2\right), \tag{2.3}$$

$$\partial_t A_\phi = (\boldsymbol{u}\times\boldsymbol{B})_\phi - \zeta_0 K j_\phi, \tag{2.4}$$

$$\partial_t B_\phi = \left[\nabla\times(\boldsymbol{u}\times\boldsymbol{B})\right]_\phi + \zeta_0 K\left(\nabla^2 B_\phi - \frac{B_\phi}{r^2}\right), \tag{2.5}$$

where ρ, T, $\boldsymbol{u}$ and $\boldsymbol{B}$ are the density, temperature, velocity and magnetic field, $\boldsymbol{B} = \nabla\times(\hat{\boldsymbol{\phi}}A_\phi) + \hat{\boldsymbol{\phi}}B_\phi$, respectively. $\boldsymbol{j}$ and τ stand for the current density and the rate of strain tensor. We have used cylindrical coordinates with $\hat{\boldsymbol{z}}$ being the vertical direction pointing downwards, $\hat{\boldsymbol{r}}$ being the radial direction and $\hat{\boldsymbol{\phi}}$ the azimuthal direction. The quantities are non-dimensionlized using the depth d of the domain as a scale for length, the sound speed at the top of the domain as a scale for velocities, and initial temperature, density, pressure and magnetic field at the top of the domain as scales for their respective quantities.

The control parameters in the simulation are the Rayleigh number at the mid-plane, R, defined as

$$R = \theta^2(m+1)\left[1 - \frac{(m+1)(\gamma-1)}{\gamma}\right]\frac{(1+\theta/2)^{2m-1}}{\sigma K^2}; \tag{2.6}$$

the Prandtl number, σ; the temperature contrast between the top and the bottom of the domain, θ; the rotation rate, Ω; the aspect ratio, the ratio between height and radius of the cylindrical domain, Γ; and the Chandrasekhar number, Q, a measure of the magnetic flux in the system defined as

$$Q = \frac{(B_0 d)^2}{\mu\rho\eta\nu}, \tag{2.7}$$

where μ the magnetic permeability, η the magnetic diffusivity, ν the kinematic viscosity, and B_0 the scale of the initial magnetic field. The ratio between specific heats is chosen to be $\gamma = 5/3$, appropriate for a monoatomic ideal gas. The initial temperature and density profiles in the simulations take the form of a polytrope, in non-dimensional form $T(z) = 1+\theta z, \rho(z) = (1+\theta z)^m$, where z and m are the non-dimensional depth (ranging

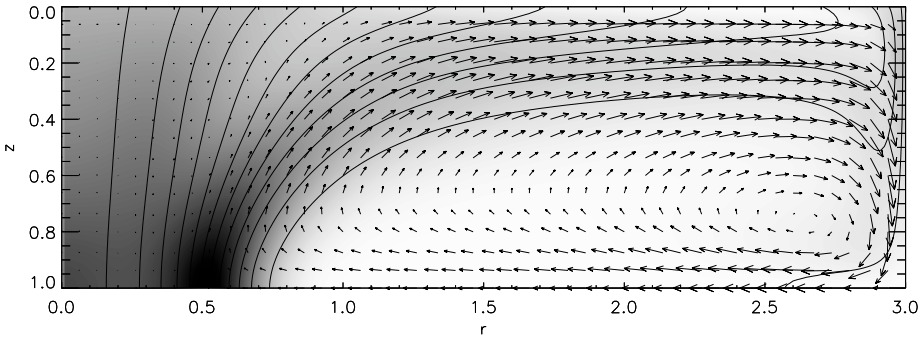

FIGURE 1. Flow velocities (arrows), magnetic field strength (gray scale, with dark indicating stronger magnetic field) and magnetic field lines for the reference case, a case that forms a diverging flow over a converging flow. See text for parameters. The rotation axis is on the left at $r = 0$.

from 0 at the top of the domain to 1 at the bottom) and the polytropic index, respectively. Simulations are started with an initial uniform vertical magnetic field $\boldsymbol{B} = \hat{\boldsymbol{z}}$ (in non-dimensional units), and are run until the system reaches a more or less steady state, if such a state can be obtained for the given set of parameters. The results presented in this paper are for aspect ratio $\Gamma = 3$.

For thermal boundary conditions, we prescribe a constant heat flux at the bottom and Stefans law at the top. The side wall is perfectly electrically conducting and does not allow for a heat flux across it. Top, bottom, and outside walls are impenetrable and stress free. The magnetic field is vertical at the bottom and matched to a potential field at the top.

The equations are solved numerically using a finite-difference scheme accurate to sixth order and a fourth-order time marching scheme.

3. Results

This work is an extension of Botha *et al.* (2006) and Botha *et al.* (2008) in which we are exploring under which conditions a stable magnetic flux concentration forms with an outflow (away from the center) over an inflow or *vice versa*. Unless otherwise specified, the simulation parameters for the results presented here are $Q = 32$, $m = 1$, $\Gamma = 3$, $\zeta_0 = 0.2$, $\Omega = 0.1$, $\sigma = 1$, $\theta = 10$, and $R = 10^5$, referred to as the reference case in the text below. This is a case in which a diverging (away from the rotation axis) over a converging flow forms. Simulation results for the same parameters were originally presented in Figure 17 of Botha *et al.* (2008). In both cases a small converging flow was prescribed as initial condition. A visualization of the flow and the magnetic field is shown here in Figure 1. Notice that the magnetic field is confined to the region near the axis where the convection flow is mostly suppressed. A stationary diverging flow exists outside of the strong magnetic field region.

Starting from this reference case, we performed a parameter study varying Prandtl number, rotation rate and, for a limited number of cases, the Chandrasekhar number. We have found that in many cases the initial conditions are important. For most parameter

Converging flow initial condition:		Prandtl number σ 0.1	0.3	1.0	2.0
Rotation rate Ω	0.00	C	C	C	D
	0.02	C	C	D	D
	0.05	C	C	D	D
	0.10	C	D	D	D

Diverging flow initial condition:		Prandtl number σ 0.03	0.1	0.3	1.0
Rotation rate Ω	0.00	X	D	D	D
	0.02	X	D	D	D
	0.05	X	D	D	D
	0.10	X	X	D	D

TABLE 1. Resulting flow configurations as a function of Prandtl number σ and rotation rate Ω. (C), tightly confined magnetic flux concentration with a converging flow around it; (D), a tightly confined magnetic flux concentration with a diverging flow around it; and (X), a configuration with poor confinement of the magnetic field according to the criterion described in the text, respectively. The left table is for the cases with an initial weak converging flow, the right side for an initial diverging flow. The other simulation parameters in all cases are $Q = 32$, $R = 10^5$, $\theta = 10$, $\gamma = 5/3$, $m = 1$, $\zeta_0 = 0.2$, and $\Gamma = 3$.

sets we therefore performed both a simulation with a weak converging circulation (flow towards the rotation axis near the top boundary and away from the axis below) and one with a weak diverging flow as initial conditions. The resulting flow configurations for Chandrasekhar number $Q = 32$ and varying Prandtl number and rotation rate are presented in table 1. The resulting configurations are classified as either a tightly confined flux tube with a diverging flow at the top, a flux tube with a converging flow near top, or as not tightly confined. Examples for these three cases are shown in Figures 1, 4 and 5, respectively.

Of course, the definition of what is a well-confined magnetic structure is somewhat arbitrary. Here, we used the following quantitative definition to determine the diameter of the magnetic field concentration around the center of the domain at the top boundary:

$$D = 2\sqrt{2\log 2 \frac{\int_0^{r_l} |\boldsymbol{B}(z=0,r)| r^2 dr}{\int_0^{r_l} |\boldsymbol{B}(z=0,r)| dr}}, \tag{3.1}$$

where r_l is the smallest radius that fulfills the condition

$$|\boldsymbol{B}(z=0,r_l) < (5/100) \max_{r<r_l}\{|\boldsymbol{B}(z=0,r)|\}. \tag{3.2}$$

This conditions makes sure that only the inner-most magnetic structure is taken into account in cases where there is additional magnetic field somewhere outside. The threshold of 5/100 is quite arbitrary but seems to work well for our purposes. We then compute the average magnetic field inside the radius $r \leq D/2$ and outside:

$$|B|_{r<D/2} = \int_0^{D/2} |\boldsymbol{B}(z=0,r)| r dr / \int_{D/2}^{\Gamma} r dr, \tag{3.3}$$

$$|B|_{r>D/2} = \int_{D/2}^{\Gamma} |\boldsymbol{B}(z=0,r)| r dr / \int_{D/2}^{\Gamma} r dr. \tag{3.4}$$

We consider the magnetic field region as tightly confined if the ratio $|B|_{r<D/2}/|B|_{r>D/2}$ is larger than 4, meaning the magnetic field inside the region is at least four times larger than the ambient field outside. Both quantities, the field strength ratio and the diameter, are plotted in Figures 2 and 3 for the cases forming tightly confined magnetic structures.

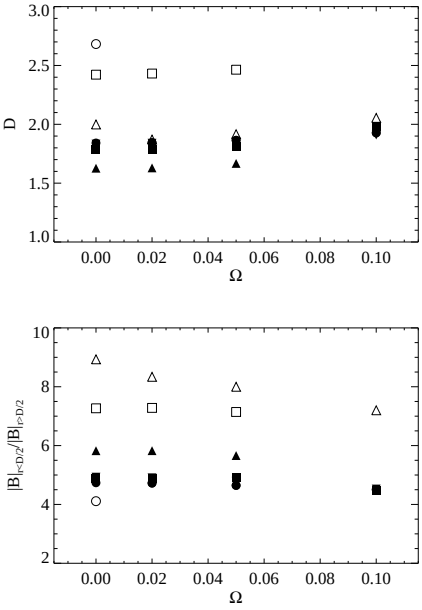

FIGURE 2. Horizontal diameter, D, of the magnetic field concentration (top panel) and ratio between mean magnetic field strength inside the field concentration and outside (bottom panel) as a function of the rotation rate Ω. The symbols correspond to Prandtl number 0.03 (diamonds), 0.1 (upward triangles), 0.3 (squares), 1.0 (circles), and 2.0 (downward triangles). Open symbols are for resulting converging flows and solid symbols for diverging flows, respectively.

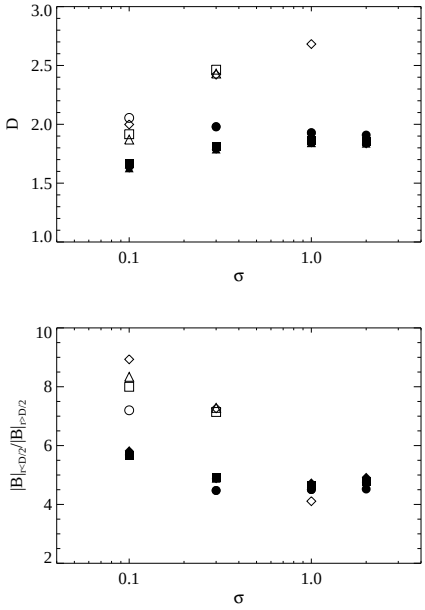

FIGURE 3. Same quantities as in the Figure on the left but as a function of Prandtl number σ. Here, the different symbols represent rotation rates 0.0 (diamonds), 0.02 (upward triangles), 0.05 (squares), and 0.1 (circles), respectively. Again, open symbols are for resulting converging flows and solid symbols for diverging flows, respectively.

The results in Table 1 show that diverging flow configurations are preferred at higher values of the rotation rate as well as the Prandtl number. At lower Prandtl numbers and/or lower rotation rate, the results depend on the initial conditions, i.e., the resulting flow is diverging if a weak diverging flow was prescribed as initial condition, and *vice versa*. Of course, the strength and size of the magnetic field concentration varies depending on the parameters of the problem. For instance, it seems intuitive that the magnetic field strength would decrease and the size would increase with increasing rotation rate, and this is indeed the case as seen in Figure 2. Although the changes are not very large, the size D does increase and the field strength ratio decreases in most cases. The dependence on the Prandtl number is shown in Figure 3. Field strength ratio decreases and structure size increases quite strongly with increasing Prandtl number. It is important to note that in all but one case converging flows produce more tightly confined magnetic structures with smaller D and larger field strength ratio.

For a small number of cases, we have also varied the value of Q which defines how much magnetic flux is in the system. The parameters for these cases are $\Omega = 0$, $\sigma = 0.03$ and

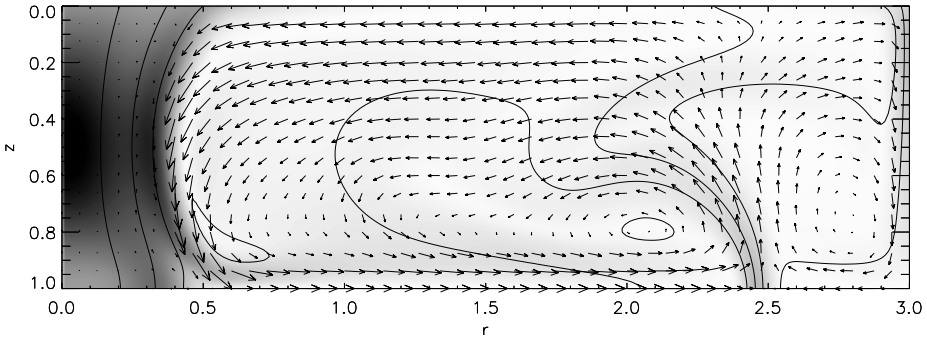

FIGURE 4. Same parameters as the reference case (Figure 1) except for $\theta = 20$ and $R = 4 \times 10^5$.

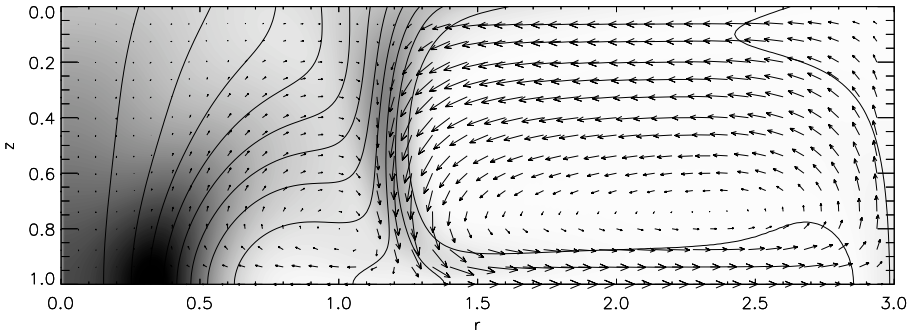

FIGURE 5. Same parameters as the reference case (Figure 1) except for rotation rate $\Omega = 0$.

$Q = 8, 16, 32, 64$ and 128. All other parameters are the same as the reference case. With increasing Chandrasekhar number Q, the field strength ratio broadly increases, but the ratio is close to or above 4 only for the highest two values of Q, i.e., a strongly confined magnetic field region realized.

Lastly, the strength of the convection, governed by the Rayleigh number R, must also play a role in the formation of magnetic field concentrations. So far, this has not been explored in detail but we can show an example for which we increased the strength of the convection compared to the reference case. Then, a converging over diverging flow as shown in Figure 4 forms instead of the diverging flow in the reference case. Instead of a single circulation, a weak secondary convective cell is formed in this case further away from the axis. The horizontal size of the magnetic field strength concentration is significantly smaller and the field strength ratio higher than in the reference case.

4. Conclusions

The simulations presented here are somewhat limited because of the simplifications and the restricted geometry, but they nevertheless can give us some insight into the

mechanisms that are involved in maintaining a tightly concentrated magnetic field near the solar surface inside structures such as magnetic pores or sunspots. Due to the simplicity of these simulations, a whole range of parameters can be explored rather easily. The simulations have shown that, depending on the parameters, stable, tightly concentrated magnetic structures can exist with both types of flow configurations: an inflow (towards the spot axis) above an outflow deeper below, or *vice versa*. In many of the studied cases, the initial conditions turned out to be important. In more realistic situations, e.g., if non-rotationally symmetric disturbances were allowed, such a strong sensitivity to initial conditions might disappear. An important result is also that for parameter sets that allow for both types of solutions, the solution with a converging flow near the surface almost always maintains a more strongly confined magnetic field with both a smaller structure size and higher ratio between the magnetic field strength inside the region and the ambient field outside.

REFERENCES

Botha, G. J. J., Busse, F. H., Hurlburt, N. E. & Rucklidge, A. M. 2008 Numerical simulations of rotating axisymmetric sunspots. *Mon. Not. R. Astron. Soc.* **387**, 1445–1462.

Botha, G. J. J., Rucklidge, A. M. & Hurlburt, N. E. 2006 Converging and diverging convection around axisymmetric magnetic flux tubes. *Mon. Not. R. Astron. Soc.* **369**, 1611–1624.

Hurlburt, N. E., Matthews, P. C. & Proctor, M. R. E. 1996 Nonlinear compressible convection in oblique magnetic fields. *Astrophys. J.* **457**, 933–+.

Hurlburt, N. E. & Rucklidge, A. M. 2000 Development of structure in pores and sunspots: flows around axisymmetric magnetic flux tubes. *Mon. Not. R. Astron. Soc.* **314**, 793–806.

Kitiashvili, I. N., Kosovichev, A. G., Wray, A. A. & Mansour, N. N. 2009 Traveling waves of magnetoconvection and the origin of the Evershed effect in sunspots. *Astrophys. J. Lett.* **700**, L178–L181.

Kitiashvili, I. N., Kosovichev, A. G., Wray, A. A. & Mansour, N. N. 2010 Mechanism of spontaneous formation of stable magnetic structures on the Sun. *Astrophys. J.* **719**, 307–312.

Rempel, M., Schüssler, M. & Knölker, M. 2009 Radiative magnetohydrodynamic simulation of sunspot structure. *Astrophys. J.* **691**, 640–649.

Zhao, J., Kosovichev, A. G. & Sekii, T. 2010 High-resolution helioseismic imaging of subsurface structures and flows of a solar active region observed by Hinode. *Astrophys. J.* **708**, 304–313.